Research Article

Jing Li, Hongjiang Ren, Jiangtao Li and Liuchang Wang*

In situ ligand synthesis affording a new Co(II) MOF for photocatalytic application

https://doi.org/10.1515/secm-2022-0229
received September 09, 2023; accepted October 20, 2023

Abstract: In situ disulfide bond formation affords a new flexible dicarboxylic acid ligand of 3,3′-dithiobisbenzoic acid (3,3′-H_2DTBA), which assembled with Co(II) ions under hydrothermal conditions, generating a novel metal–organic framework (MOF), namely, $[Co(3,3'\text{-}DTBA)_2(H_2O)_2]_n$ (**1**). This compound is assembled from layered structures, featuring weak interlayer interactions that can reduce pore blockage through relative sliding. The results of photocatalytic experiment indicate that MOF **1** is a good semiconducting material and it can function as photocatalyst for degrading methylene blue under the ultraviolet light irradiation. Cyclic experiments demonstrated its good stability and long-lasting photocatalytic performance, indicating its potential application value.

Keywords: hydrothermal conditions, MOF, photocatalysis, semiconducting material, UV light irradiation

1 Introduction

The development of metal–organic frameworks (MOFs) has experienced an explosive growth driven by their multiple functional properties in different application fields such as gas storage, luminescence sensing, heterogeneous catalysis, magnetism, biomedicine, electrode materials, and energy storage devices [1–9]. These MOF materials with different extended network structures are generally constructed by the coordination bond-driven self-assembly reactions of metal ions and organic bridging ligands. A large number of reports about MOFs have demonstrated that carboxylate ligands are one of the most popular organic ligands for the preparing MOF materials due to their excellent coordination capacities to metal centers and abundant coordination modes [10–13]. The commonly used organic ligands can be commercially available or presynthesized, whose structures can be captured in the MOFs. However, there are also some MOFs with the organic ligands that are not used in the raw materials, indicating that appropriate organic ligand can experience in situ reaction to form new organic ligand under hydro-(solvo)thermal conditions. In the field of MOFs synthesis, the in situ ligand formation reactions consist of C–C bond formation or cleavage, alkylation, hydroxylation, and decarboxylation of aromatic benzene ring, hydrolysis, cycloaddition of organic nitrile, S–S bond formation, and so on, which afforded lots of MOFs with novel topological structures and application properties that cannot be obtained by the direct preparation [14–19]. Based on the reported studies, 3-mercaptobenzoic acid (3-HMBA) can be transformed into 3,3′-dithiobisbenzoic acid (3,3′-H_2DTBA) via the in situ disulfide bond formation, which further self-assemble with metal ions to construct new MOFs [20]. Using this in situ disulfide bond formation reaction, we selected, in this work, 3-HMBA as the starting organic block and let it react with Co(II) ions under a hydrothermal condition. Then, we obtained a new MOF. An X-ray analysis on structure shows that MOF **1** demonstrates a 0D isolated structure, which extended into a 2D supramolecular layer via the intermolecular hydrogen bonds. The layered structure can further stack into a 3D structure under the influence of van der Waals forces. Due to the weaker interlayer forces, the relative sliding between layers offers a potential solution to the catalyst deactivation issue often encountered in conventional 3D large pore structures caused by pore blockage.

Methylene blue (MB) is easily detectable in experiments due to its distinctive absorption and emission spectra. Its structure is relatively stable and does not undergo spontaneous degradation, ensuring reliable experimental results. Furthermore, MB is representative of a large class of organic pollutants because of its aromatic structures and double bonds. Thus, MB is commonly used as a substrate

*** Corresponding author: Liuchang Wang,** The Key Laboratory for Surface Engineering and Remanufacturing in Shaanxi Province, Key Laboratory of Chemistry of New Material of Functional Inorganic Composites, School of Chemical Engineering, Xi'an University, Xi'an, Shaanxi, China, e-mail: wlg_112@163.com
Jing Li, **Hongjiang Ren**, **Jiangtao Li:** The Key Laboratory for Surface Engineering and Remanufacturing in Shaanxi Province, Key Laboratory of Chemistry of New Material of Functional Inorganic Composites, School of Chemical Engineering, Xi'an University, Xi'an, Shaanxi, China

in photocatalytic degradation experiments to study the performance of photocatalytic materials. In order to further investigate the photocatalytic performance of MOF **1**, this study used MB as a substrate for photocatalytic degradation experiments. The results demonstrate its excellent photocatalytic activity in degrading MB. Moreover, cyclic experiments have confirmed the stability of its structure and its reusability. These experiments collectively illustrate that MOF **1**, as a catalyst for the photocatalytic degradation of MB, holds high potential for practical applications.

2 Experimental

2.1 Materials and instrumentation

The raw materials for the preparing of MOF **1** are all of analytical grade and can be commercially available. Analysis on elements of C and H was conducted using the EA-1110 elemental analyzer. The pattern of powder X-ray diffraction (PXRD) of MOF **1** was recorded using a Rigaku D/Max-2500 PC diffractometer. Thermogravimetric analysis (TGA) experiment was performed using NETSCHZ STA-449C thermoanalyzer under a constant flow of air from 30 to 800°C.

2.2 Synthesis of $[Co(3,3'\text{-}DTBA)_2(H_2O)_2]_n$ (1)

A mixture of $Co(NO_3)_2{\cdot}6H_2O$ (0.100 mmol), 3-HMBA (0.1 mmol), and H_2O (1.0 mL) was put into a 25 mL Teflon-coated, stainless steel container. Then, the container were sealed and incubated at 150°C for 72 h. Then, the container was cooled to the ordinary room temperature with the cooling rate of 2°C/min, purple crystal blocks were generated, and their yield is 42% based on 3-HMBA. Elemental analysis calcd. for $C_{28}H_{22}CoO_{10}S_4$ (705.63): C, 47.62; H, 3.12%. Found: C, 47.59; H, 3.15%.

2.3 X-ray structural determination

A single crystal of MOF **1** for X-ray diffraction analysis was selected via optical microscope and glued onto a piece of glass fiber. The structural data of MOF 1 was detected by a Rigaku Mercury CCD diffractometer and the Mo-Kα radiation by graphite monochromator at 293 K. The structure was then solved using the direct methods and refined by the full-matrix least-squares method based F^2 values using OLEX2 program [21]. Non-hydrogen atoms were refined in an anisotropic manner; meanwhile, the hydrogen atoms attached to carbon atoms and water molecules were fixed at their geometrical positions. Data on crystallography and refinements for **1** are listed in Table 1.

Table 1: Crystal data for compound **1**

Formula	$C_{28}H_{22}CoO_{10}S_4$
Fw	705.63
Crystal system	Triclinic
Space group	*P*-1
a (Å)	7.046(4)
b (Å)	7.331(4)
c (Å)	15.415(7)
α (°)	90.5210(10)
β (°)	93.110(8)
γ (°)	115.242(7)
Volume (Å^3)	718.7(6)
Z	1
Density (calculated)	0.946
Abs. coeff. (mm^{-1})	1.630
Total reflections	5,582
Unique reflections	3,063
Goodness of fit on F^2	1.076
Final *R* indices [$I > 2\text{sigma}(I^2)$]	$R = 0.0455$, $wR_2 = 0.1276$
R (all data)	$R = 0.0536$, $wR_2 = 0.1360$

3 Results and discussion

3.1 Crystal structure of MOF 1

Using single-crystal X-ray diffraction characterization, MOF **1** crystallizes in the *P*-1 space group of triclinic system. The asymmetric unit of **1** consists of one Co(II) ions, one in situ generated 3,3′-DTBA^{2-} ligand, and one coordinated water molecule. As you can see in Figure 1a, Co1 ion is hexa-coordinated by two terminal water ligands, as well as four carboxyl O atoms from two different HL^- ligands, generating a slightly distorted octahedron of $\{CoO_6\}$ with the Co–O bond distances spanning from 2.133(2) to 2.173(3) Å. Thanks to the in situ generated disulfide bond, two independent 3,3′-DTBA^{2-} ligands in the *cis* conformation chelate one Co(II) center to form a 0D isolated structure (Figure 1b). In this 0D structure, four carboxyl O atoms defined the equatorial plane of the $\{CoO_6\}$ octahedron, and the apical positions of the $\{CoO_6\}$ octahedron are occupied by two terminal water ligands. The H donors from the coordinated water molecules in the 0D isolated structure can be taken

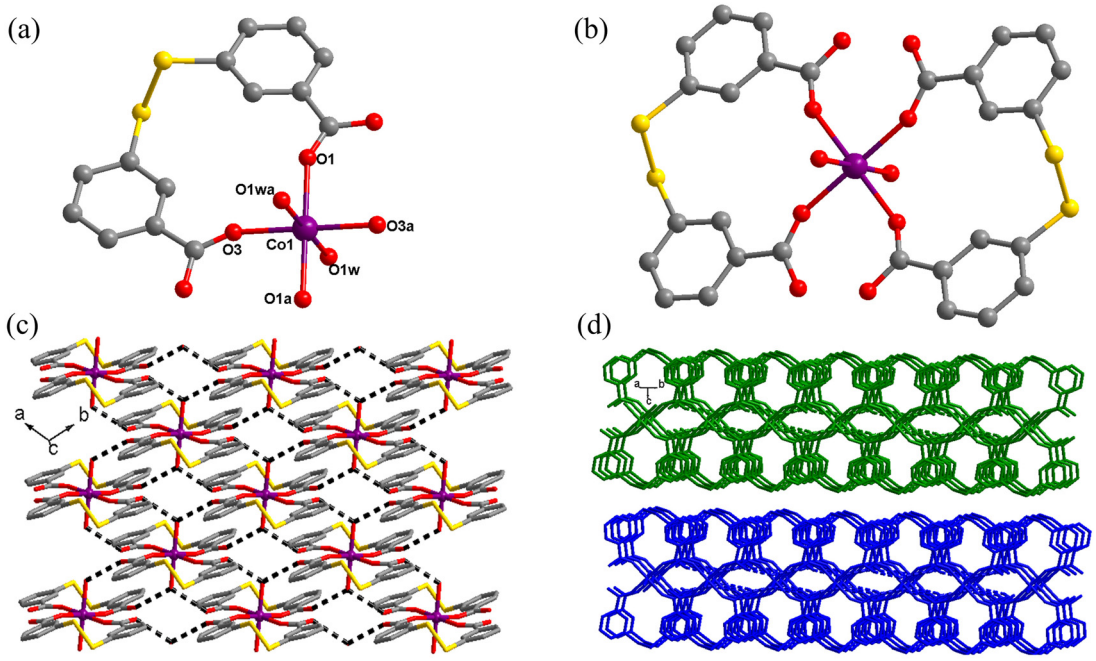

Figure 1: (a) View of the coordination environments of Co(II) ion in **1**, (b) the 0D isolated structure of **1**, (c) intermolecular hydrogen bonds constructed 2D layer for **1**, and (d) the piled-up 3D supramolecular framework for **1**.

in by the carboxyl O atoms from OD isolated structures nearby, forming intermolecular hydrogen bonds (O1w-H1wa…O4 = 2.8396 Å and O1w-H1wa…O2 = 2.7611 Å), which extended these structures into a 2D layered motif (Figure 1c). Finally, these 2D layered motifs piled up under the guidance of weak van der Waals forces, affording a 3D supramolecular framework as displayed in Figure 1d. Due to the weak interlayer interactions in this 3D framework, relative sliding can easily occur. This interesting structural feature holds promise as a feasible solution to the issue of catalyst deactivation caused by pore blockage, often encountered in conventional 3D macroporous structures.

3.1.1 Pattern of PXRD and TGA

The PXRD experiment result is demonstrated in Figure 2a. Obviously, the pattern of the fabricated bulk samples is in good match with that simulated from the single-crystal structure data, indicating the good phase purity of the experimentally prepared sample. Besides, the PXRD pattern of the recovered sample after photocatalytic experiments is also consistent with the simulated pattern of single-crystal X-ray diffraction. This indicates the integrity of the recovered sample after photocatalytic experiments. In other words, photocatalytic experiments do not affect the fundamental structural characteristics and properties of the sample, demonstrating that the material functions as a photocatalyst with good stability and potential applications.

Besides, we also investigated the thermostability of MOF **1** under a constant flow of air from 30 to 800°C (Figure 2b). In the range of 95–120°C, the weight loss is 5.04%, similar to the release of the coordinated water molecules (calcd: 5.10%). From 120 to 290°C, it can be seen a stable platform, indicating that the skeleton structure of **1** can be stabilized to 290°C. Beyond 290°C, the skeleton structure collapsed with a clear weight loss that attributed to the combustion of organic ligand.

3.2 Optical band gap and photocatalytic property of MOF 1

Based on the ultraviolet (UV)–visible absorption spectrum of MOF **1**, its optical band gap, which is an important indicator to evaluate a semiconductive material, can be calculated to be 3.15 eV via the Kubelka–Munk function (Figure 3a), indicating that MOF **1** may be a photocatalyst suitable for the degradation of dye contaminants.

The reports indicate that Co(II)-based MOFs usually exhibit excellent photocatalytic activity when it concerns the degradation of organic dyes under UV light irradiation [22,23].

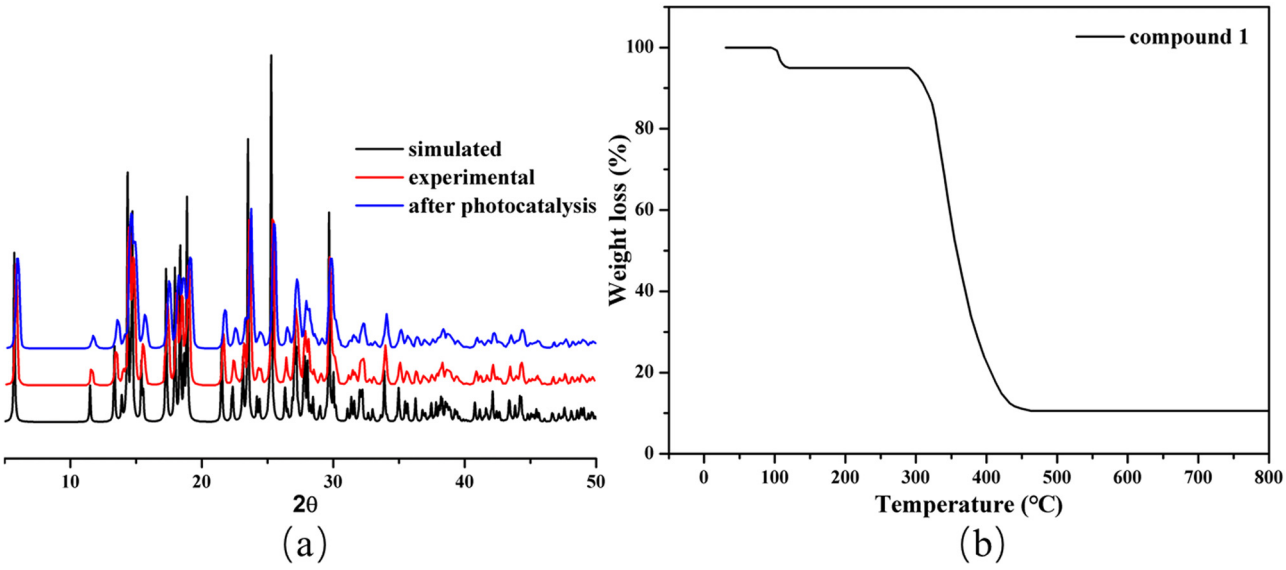

Figure 2: (a) PXRD patterns for 1 and (b) the TGA curve of 1.

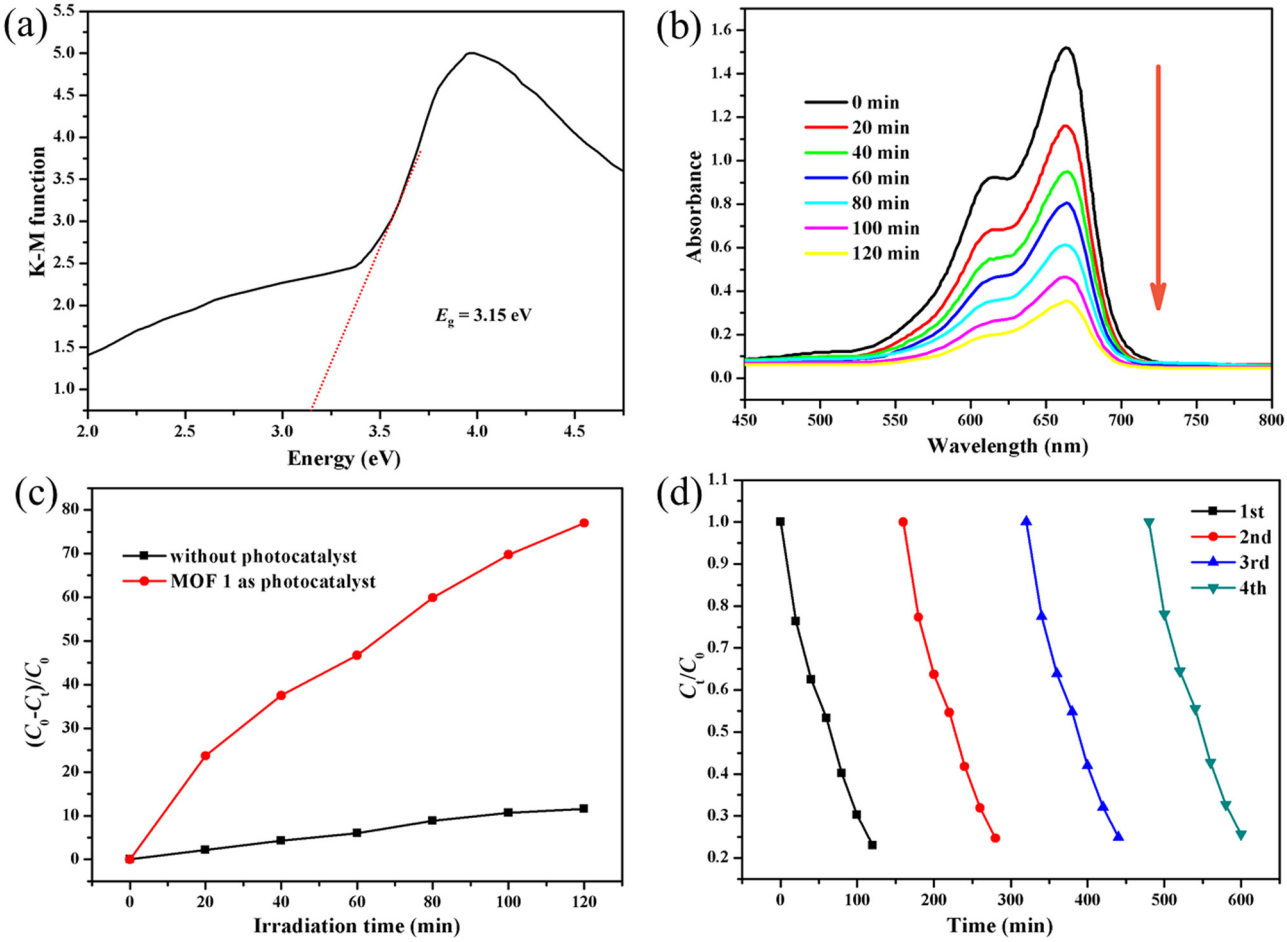

Figure 3: (a) Spectrum of MOF **1** about the Kubelka–Munk transformed diffuse reflectance, (b) the UV–visible absorption spectra of MB in the presence of **1** under UV light irradiation, (c) the plots of degradation efficiency in the presence of **1** or without any photocatalyst, and (d) recycle runs of the photocatalytic degradation of MB in the presence of **1**.

To estimate the photocatalytic property of MOF **1**, this work selected MB as a model dye for the photodegradation experiments. About 30 mg of powder samples of MOF **1** was dispersed into a MB aqueous solution at a concentration level of 10 mg/L, and in the dark, the suspension underwent a 60 min ultrasonic bath to realize the equilibrium between absorption and desorption. Then, the suspension was continuously exposed to UV light. About 5 mL of the reaction mixture was stored for regular intervals and centrifuged to remove the solid photocatalyst. The characteristic absorption peak at 664 nm for MB was chosen to observe the photocatalytic process. As shown in Figure 3b, the absorption peak at 664 nm dropped obviously as it was exposed longer to UV light, and the degradation efficiency of MB is 76.97% after 120 min of UV irradiation (Figure 3c). As there is no photocatalyst, the degradation efficiency of MB is only 11.56% when the irradiation time is the same (Figure 3c). Evidently, such experiment results demonstrated the good photocatalytic activity of MOF **1**. The stability of such photocatalyst was also investigated *via* the cycle experiments. As we could discover in Figure 3d, the efficiency of MB degradation exhibited no obvious decrease after the fourth cycle experiment. The powder samples after the fourth cycle experiment were collected and further used to perform the PXRD experiment under room temperature (Figure 2a). The PXRD pattern after photocatalysis exhibits no obvious change compared to that of pristine sample, which indicates that the MOF **1** has a good structural stability during the photocatalytic process.

4 Conclusion

In a nutshell, we have obtained a new Co(II) MOF via the in situ ligand synthesis and hydrothermal self-assembly reaction. Analysis of X-ray crystallography demonstrated the 0D isolated structure of MOF **1**. Intermolecular hydrogen bonds further combined these 0D isolated units together, extending to a 2D layered motif. The weak interlayer interactions, leading to the property of relative sliding, contribute to its long-lasting photocatalytic activity. Benefiting from its good semiconducting property, MOF **1** shows excellent photocatalytic activity as to the degradation of dye contaminant MB under the light illumination of UV.

Funding information: The research was supported by Research on the Application of Inorganic Nanofunctional Composite Materials (XAWLKYTD202312), Natural Science Basic Research Plan in Shaanxi Province of China (2022JM-075), and Three-Year Action Plan Project of Xi'an University (21XJZZ0001-11).

Author contributions: Jing Li and Liuchang Wang synthesized and characterized the compounds; Hongjiang Ren and Jiangtao Li performed other experiments.

Conflict of interest: The authors state no conflict of interest.

Data availability statement: The data used to support the findings of this study are included within the article.

Ethical approval: Research experiments conducted in this article with animals or humans were approved by the ethical committee and responsible authorities of our research organization(s) following all guidelines, regulations, legal, and ethical standards as required for humans or animals.

References

[1] Allendorf MD, Bauer CA, Bhakta RK. Luminescent metal-organic frameworks. Chem Soc Rev. 2009;38:1330–52.
[2] Lee J, Farha QK, Roberts J, Scheidt KA, Nguyen ST, Hupp JT. Metal-organic framework materials as catalysts. Chem Soc Rev. 2009;38:1450–9.
[3] Seth S, Savitha G, Moorthy JN. Carbon dioxide capture by a metal-organic framework with nitrogen-rich channels based on rationally designed triazole-functionalized tetraacid organic linker. Inorg Chem. 2015;54:6829–35.
[4] Pei RB, Cao MY, Li LK, Dong XY, Zang SQ. A series of transition metal-organic frameworks based on a bipyridinium carboxylate ligand: Syntheses, structures and photoluminescent properties. J Mol Struct. 2017;1143:72–83.
[5] Ghasempour H, Wang KY, Powell JA, Zarekarizi F, Lv XL, Morsali A, et al. Metal-organic frameworks based on multicarboxylate linkers. Coord Chem Rev. 2021;426:213542.
[6] Zhang Y, Liu Y, Liu Z, Wu X, Wen Y, Chen H, et al. MnO_2 cathode materials with the improved stability *via* nitrogen doping for aqueous zinc-ion batteries. J Energy Chem. 2022;64:23–32.
[7] Parveen N, Ansari SA, Ansari MZ, Ansari MO. Manganese oxide as an effective electrode material for energy storage: a review. Environ Chem Lett. 2022;20:283–309.
[8] Abbas N, Shaheen I, Hussain I, Lamiel C, Ahmad M, Ma X, et al. Glycerol-mediated synthesis of copper-doped zinc sulfide with ultrathin nanoflakes for flexible energy electrode materials. J Alloys Compd. 2022;919:165701.
[9] Hussain I, Ansari MZ, Lamiel C, Hussain T, Javed MS, Kaewmaraya T, et al. *In situ* grown heterostructure based on MOF-derived carbon containing n-Type Zn–In–S and dry-oxidative p-Type CuO as pseudocapacitive electrode materials. ACS Energy Lett. 2023;8:1887–95.

[10] An YY, Liu LP, Zhu ML. Construction of a new (4,8)-connected coordination polymer based on the zinc cluster: structure, topology, and luminescence. Chin J Struct Chem. 2018;37:1479–85.
[11] Zhang J, Chen S, Bu X. Multiple functions of ionic liquids in the synthesis of 3-D low-connectivity homochiral and achiral frameworks. Angew Chem Int Ed. 2008;47:5434–7.
[12] Wang Y, Yang GP, Zhang PF, Ma LL, Wang JM, Li GP, et al. Microporous Cd(II) metal-organic framework for CO_2 catalysis, luminescent sensing, and absorption of methyl green. Cryst Growth Des. 2021;21:2734–43.
[13] Chen YQ, Zhai JX, Tian Y, Liu XP. Auxiliary ligand oriented Cd(II)-flexible dicarboxylic acid coordination frameworks: syntheses, structures and properties. Chin J Struct Chem. 2019;38:1311–9.
[14] Weng Z, Xiang P, Ling J, Huang M, Yang W, Zheng Z, et al. *In situ* synthesis and characterization of a series of new pyridyl containing complexes based on 3d metals: from oligomer to 3D framework. J Solid State Chem. 2020;287:121326.
[15] Zhang L, Li ZJ, Qin YY, Zhang J, Cheng JK, Yin PX, et al. pH-controlled assembly of two supramolecular architectures based on Cu(II)-metallacycle building blocks. J Mol Struct. 2008;891:138–42.
[16] Yuan N, Sheng T, Zhang J, Tian C, Hu S, Huang X, et al. A disulfide ligand with axial chirality generated *in situ* for the construction of an unusual hxg topological coordination polymer. CrystEngComm. 2011;13:5951–5.
[17] Lin L, Zhang X, Zhang J, Yao YG. Hydrothermal *in situ* ligand synthesis and chiral self-assembly with Pr(III). J Mol Struct. 2011;1006:83–6.
[18] Chen F, Wu MF, Liu GN, Wang MS, Zheng FK, Yang C, et al. Zinc(II) and cadmium(II) coordination polymers based on 3-(5H-tetrazolyl) benzoate ligand with different coordination modes: hydrothermal syntheses, crystal structures and ligand-centered luminescence. Eur J Inorg Chem. 2010;31:4982–91.
[19] Dong R, Chen X, Li Q, Hu M, Huang L, Li C, et al. (1H-tetrazol-5-yl) methyl) pyridine-based metal coordination complexes: *in situ* tetrazole synthesis, crystal structures, luminescence properties. CrystEngComm. 2015;17:1305–17.
[20] Rowland CE, Belai N, Knope KE, Cahill CL. Hydrothermal synthesis of disulfide-containing uranyl compounds: *in situ* ligand synthesis versus direct assembly. Cryst Growth Des. 2010;10:1390–8.
[21] Sheldrick GM. Crystal structure refinement with SHELXL. Acta Crystallogr. Sect C: Struct Chem. 2015;71:3–8.
[22] Wang XF, Guo XY, Liu T. Two Co(II) based coordination polymers constructed from π-electron rich polycarboxylate aryl ether ligand: structural insights and photocatalytic dye degradation. Chin J Struct Chem. 2021;6:722–8.
[23] Zhang D, Bi C, Zong Z, Fan Y. Three different Co(II) metal–organic frameworks based on 4,4′-bis(imidazolyl)diphenyl ether: syntheses, crystal structure and photocatalytic properties. J Inorg Organomet Poly. 2020;30:5148–56.